Numerical analysis of superconducting phases in the extended Hubbard model with non-local pairing

University of Pisa, a.y. 2025-2026

Alessandro Gori*

Thesis for the Master's degree in Physics

Abstract

[To be continued...]

Contents

Draft: December 20, 2025

*a.gori23@studenti.unipi.it / nepero27178@github.com

List of symbols and abbreviations

AF	Anti-Ferromagnetic
BCS	Bardeen-Cooper-Schrieffer (theory)
DoF	Degree of Freedom
HF	Hartree-Fock
MFT	Mean-Field Theory
SC	Superconductor
T_c	Critical temperature

Part I

Mean-Field-Theory analysis

Chapter 1

Mean-Field Theory in Hubbard lattices

In this Appendix the MFT solutions to the conventional Hubbard hamiltonian of Eq. (**??**),

$$\hat{H} = -t \sum_{\langle ij \rangle} \sum_{\sigma} \hat{c}^{\dagger}_{i\sigma} \hat{c}_{j\sigma} + U \sum_{i} \hat{n}_{i\uparrow} \hat{n}_{i\downarrow} \qquad t, U > 0 \tag{1.1}$$

are described. The discussion is limited to the two-dimensional square lattice.

1.1 Symmetries of the Hubbard model and magnetic phase transitions

The Hubbard model defined on the planar square lattice presents various natural symmetries, discussed in detail by Arovas et al. [1] and for the EHM in Sec. **??**. These are reported in Tab. **??**. For the conventional Hubbard model, $\hat{H}_t + \hat{H}_U$, the three essential symmetries are translational invariance, spin rotations and charge conservation. In this appendix we investigate magnetic ordering: thus we perform a SU(2) $\rightarrow$ U(1) SSB of the kind depicted in Fig. **??**, choosing a particular magnetization direction.

As is done in Chap. **??**, the starting point is to apply Wick's theorem to reduce the quartic hamiltonian of Eq. (1.1) to a quadratic form. Considering the discussion that leads to Eq. (**??**), it's evident that for the symmetry scheme we are dealing with the Fock term in decomposition is always suppressed, as well as the Cooper term. Then we remain with just the Hartree term,

$$\begin{aligned} \hat{n}_{i\uparrow} \hat{n}_{i\downarrow} &= \left(\langle \hat{n}_{i\uparrow} \rangle + \delta \hat{n}_{i\uparrow} \right) \left(\langle \hat{n}_{i\downarrow} \rangle + \delta \hat{n}_{i\downarrow} \right) \\ &\simeq \langle \hat{n}_{i\uparrow} \rangle \langle \hat{n}_{i\downarrow} \rangle + \delta \hat{n}_{i\uparrow} \langle \hat{n}_{i\downarrow} \rangle + \langle \hat{n}_{i\uparrow} \rangle \delta \hat{n}_{i\downarrow} + \mathcal{O}\left(\delta n^2 \right) \\ &= - \langle \hat{n}_{i\uparrow} \rangle \langle \hat{n}_{i\downarrow} \rangle + \hat{n}_{i\uparrow} \langle \hat{n}_{i\downarrow} \rangle + \langle \hat{n}_{i\uparrow} \rangle \hat{n}_{i\downarrow} + \mathcal{O}\left(\delta n^2 \right) \end{aligned}$$

where $\delta \hat{n}_{i\sigma} \equiv \hat{n}_{i\sigma} - \langle \hat{n}_{i\sigma} \rangle$ and orders higher than first have been ignored, assuming negligible fluctuations around the equilibrium single-site population. The first term of the above three can be neglected at fixed particles number, being a pure energy shift.

1.2 Ferromagnetic phase

The MFT ferromagnetic solution prescribes an uniformly magnetized lattice,

$$\langle \hat{n}_{i\uparrow} \rangle = n + m \qquad \langle \hat{n}_{i\downarrow} \rangle = n - m$$

where n is the site electron density and m is the density unbalance, leading to a magnetization per site $2m$. The mean-field hamiltonian with these substitutions becomes:

$$\begin{aligned} \hat{H} &\simeq -t \sum_{\langle ij \rangle} \sum_{\sigma} \hat{c}^{\dagger}_{i\sigma} \hat{c}_{j\sigma} + U \sum_{i} \left[\hat{n}_{i\uparrow} \langle \hat{n}_{i\downarrow} \rangle + \langle \hat{n}_{i\uparrow} \rangle \hat{n}_{i\downarrow} \right] \\ &= -t \sum_{\langle ij \rangle} \sum_{\sigma} \hat{c}^{\dagger}_{i\sigma} \hat{c}_{j\sigma} + nU \sum_{i} \left[\hat{n}_{i\uparrow} + \hat{n}_{i\downarrow} \right] - mU \sum_{i} \left[\hat{n}_{i\uparrow} - \hat{n}_{i\downarrow} \right] \end{aligned}$$

Figure 1.1 | Depiction of the Hubbard square lattice hopping band $\epsilon_{\mathbf{k}} = -2t[\cos(k_x) + \cos(k_y)]$. The red lines mark the zero-energy intersection.

Fourier transforming,

$$-t \sum_{\langle ij \rangle} \sum_{\sigma} \hat{c}^{\dagger}_{i\sigma} \hat{c}_{j\sigma} = -2t \sum_{\mathbf{k}\sigma} \left[\cos(k_x) + \cos(k_y)\right] \hat{n}_{\mathbf{k}\sigma}$$
$$nU \sum_{i} \left[\hat{n}_{i\uparrow} + \hat{n}_{i\downarrow}\right] = nU \sum_{\mathbf{k}\sigma} \hat{n}_{\mathbf{k}\sigma}$$
$$mU \sum_{i} \left[\hat{n}_{i\uparrow} - \hat{n}_{i\downarrow}\right] = mU \sum_{\mathbf{k}\sigma} \left[\hat{n}_{\mathbf{k}\uparrow} - \hat{n}_{\mathbf{k}\downarrow}\right]$$

For a square lattice, the Brillouin Zone is delimited by

$$\mathbf{k} \in [-\pi, \pi] \times [-\pi, \pi]$$

The hopping single-state energy is given by

$$\epsilon_{\mathbf{k}} = -2t \left[\cos(k_x) + \cos(k_y)\right]$$

represented as a band in Fig. 1.1. At $U = 0$, the mean-field ferromagnetic state fills the band bottom-up. The single-state energy becomes:

$$\epsilon_{\mathbf{k}\uparrow} = U\,(n - m) - 2t \left[\cos(k_x) + \cos(k_y)\right]$$
$$\epsilon_{\mathbf{k}\downarrow} = U\,(n + m) - 2t \left[\cos(k_x) + \cos(k_y)\right]$$

Now it is a matter of finding the optimal value for m, minimizing the total energy at fixed filling $\rho = 2n$. Notice that said minimization is performed parametrically varying the magnetization m, inside the ferromagnetic-polarized space. As it turns out, for strong local repulsion $U/t \gg 1$, antiferromagnetic ordering is preferred. Comparison is needed in order to assess which magnetic ordering is preferred.

Consider the half-filling situation. An unpolarized system will have $n = 1/4$, $m = 0$: this implies $\langle \hat{n}_{i\uparrow} \rangle = \langle \hat{n}_{i\downarrow} \rangle = 1/4$. A perfectly up-ferromagnetic system, $n = 1/4$, $m = 1/4$: then $\langle \hat{n}_{i\uparrow} \rangle = 1/2$ and $\langle \hat{n}_{i\downarrow} \rangle = 0$. [To be continued...]

1.3 Antiferromagnetic phase

Consider now an AF mean-field solution. Let us change notation, indicating each site as

$$i \to \mathbf{r} = (x, y) \qquad x, y \in \mathbb{N}$$

The mean-field AF solution at half-filling is the uniform-modulated magnetization

$$m_{\mathbf{r}} = (-1)^{x+y} m \qquad m \in [-1, 1]$$

and a mean-field Ansatz

$$\langle \hat{n}_{\mathbf{r}\uparrow} \rangle = n + m_{\mathbf{r}} \qquad \langle \hat{n}_{\mathbf{r}\downarrow} \rangle = n - m_{\mathbf{r}} \tag{1.2}$$

In next sections, the details of the MFT solution are discussed.

1.3.1 MFT discussion

With respect to the ferromagnetic solution presented above, the only detail changing is the last term,

$$\hat{H} = -t \sum_{\langle \mathbf{r}\mathbf{r}' \rangle} \sum_{\sigma} \hat{c}^{\dagger}_{\mathbf{r}\sigma} \hat{c}_{\mathbf{r}'\sigma} + nU \sum_{\mathbf{r}} \left[\hat{n}_{\mathbf{r}\uparrow} + \hat{n}_{\mathbf{r}\downarrow}\right] - mU \sum_{\mathbf{r}} (-1)^{x+y} \left[\hat{n}_{\mathbf{r}\uparrow} - \hat{n}_{\mathbf{r}\downarrow}\right] \tag{1.3}$$

Figure 1.2 | Alternative depiction of the Hubbard square lattice hopping band previously reported in Fig. 1.1. The Magnetic Brillouin Zone (MBZ) is delimited by the zero-energy contour and is indicated in figure. As it is evident, energy sign flips by taking a (π, π) translation in $\mathbf{k}$ space.

Fourier-transforming, the phase factor can be absorbed in the destruction operator inside of $\hat{n}_{\mathbf{r}\sigma}$:

$$\begin{aligned}\sum_{\mathbf{r}}(-1)^{x+y}\hat{n}_{\mathbf{r}\sigma} &= \sum_{\mathbf{r}}(-1)^{x+y}\hat{c}^{\dagger}_{\mathbf{r}\sigma}\hat{c}_{\mathbf{r}\sigma}\\ &= \sum_{\mathbf{r}} e^{i\boldsymbol{\pi}\cdot\mathbf{r}}\frac{1}{\sqrt{L_xL_y}}\sum_{\mathbf{k}\in\mathrm{BZ}} e^{i\mathbf{k}\cdot\mathbf{r}}\hat{c}^{\dagger}_{\mathbf{k}\sigma}\frac{1}{\sqrt{L_xL_y}}\sum_{\mathbf{k}'\in\mathrm{BZ}} e^{-i\mathbf{k}'\cdot\mathbf{r}}\hat{c}_{\mathbf{k}'\sigma}\\ &= \sum_{\mathbf{k}\in\mathrm{BZ}}\sum_{\mathbf{k}'\in\mathrm{BZ}}\hat{c}^{\dagger}_{\mathbf{k}\sigma}\hat{c}_{\mathbf{k}'\sigma}\frac{1}{L_xL_y}\sum_{\mathbf{r}} e^{-i[\mathbf{k}'-(\mathbf{k}+\boldsymbol{\pi})]\cdot\mathbf{r}}\\ &= \sum_{\mathbf{k}\in\mathrm{BZ}}\hat{c}^{\dagger}_{\mathbf{k}\sigma}\hat{c}_{\mathbf{k}+\boldsymbol{\pi}\sigma}\end{aligned}$$

where $\boldsymbol{\pi} = (\pi, \pi)$. It follows:

$$mU\sum_{\mathbf{r}}(-1)^{x+y}\left[\hat{n}_{\mathbf{r}\uparrow} - \hat{n}_{\mathbf{r}\downarrow}\right] = \Delta\sum_{\mathbf{k}\in\mathrm{BZ}}\left[\hat{c}^{\dagger}_{\mathbf{k}\uparrow}\hat{c}_{\mathbf{k}+\boldsymbol{\pi}\uparrow} - \hat{c}^{\dagger}_{\mathbf{k}\downarrow}\hat{c}_{\mathbf{k}+\boldsymbol{\pi}\downarrow}\right] \quad \text{where} \quad \Delta \equiv mU$$

Consider the band of Fig. 1.1 at half-filling. As does Fabrizio [4], the area delimited externally by the solid lines at zero energy is denominated "Magnetic Brillouin Zone" (MBZ). The periodicity of $\mathbf{k}$ space guarantees that the full BZ can be taken as well to be the one of Fig. **??**. Then:

$$\begin{aligned}\sum_{\mathbf{k}\in\mathrm{BZ}}\hat{c}^{\dagger}_{\mathbf{k}\uparrow}\hat{c}_{\mathbf{k}+\boldsymbol{\pi}\uparrow} &= \sum_{\mathbf{k}\in\mathrm{MBZ}}\left[\hat{c}^{\dagger}_{\mathbf{k}\uparrow}\hat{c}_{\mathbf{k}+\boldsymbol{\pi}\uparrow} + \hat{c}^{\dagger}_{\mathbf{k}+\boldsymbol{\pi}\uparrow}\hat{c}_{\mathbf{k}+2\boldsymbol{\pi}\uparrow}\right]\\ &= \sum_{\mathbf{k}\in\mathrm{MBZ}}\left[\hat{c}^{\dagger}_{\mathbf{k}\uparrow}\hat{c}_{\mathbf{k}+\boldsymbol{\pi}\uparrow} + \hat{c}^{\dagger}_{\mathbf{k}+\boldsymbol{\pi}\uparrow}\hat{c}_{\mathbf{k}\uparrow}\right]\end{aligned} \tag{1.4}$$

and the same applies for spin $\downarrow$. Periodicity by shifts $2\boldsymbol{\pi}$ has been used. Now, define the Nambu spinors:

$$\hat{\Psi}_{\mathbf{k}\sigma} \equiv \begin{bmatrix}\hat{c}_{\mathbf{k}\sigma}\\ \hat{c}_{\mathbf{k}+\boldsymbol{\pi}\sigma}\end{bmatrix}$$

and a spin-wise gap,

$$\Delta_{\uparrow} = \Delta \qquad \Delta_{\downarrow} = -\Delta$$

At fixed filling, the nU term is a pure chemical potential shift, thus will be neglected. The kinetic term transforms as

$$\begin{aligned}-t\sum_{\langle ij\rangle}\sum_{\sigma}\hat{c}^{\dagger}_{i\sigma}\hat{c}_{j\sigma} &= \sum_{\mathbf{k}\in\mathrm{BZ}}\sum_{\sigma}\epsilon_{\mathbf{k}}\hat{c}^{\dagger}_{\mathbf{k}\sigma}\hat{c}_{\mathbf{k}\sigma}\\ &= \sum_{\mathbf{k}\in\mathrm{MBZ}}\sum_{\sigma}\left[\epsilon_{\mathbf{k}}\hat{c}^{\dagger}_{\mathbf{k}\sigma}\hat{c}_{\mathbf{k}\sigma} + \epsilon_{\mathbf{k}+\boldsymbol{\pi}}\hat{c}^{\dagger}_{\mathbf{k}+\boldsymbol{\pi}\sigma}\hat{c}_{\mathbf{k}+\boldsymbol{\pi}\sigma}\right]\\ &= \sum_{\mathbf{k}\in\mathrm{MBZ}}\sum_{\sigma}\epsilon_{\mathbf{k}}\left[\hat{c}^{\dagger}_{\mathbf{k}\sigma}\hat{c}_{\mathbf{k}\sigma} - \hat{c}^{\dagger}_{\mathbf{k}+\boldsymbol{\pi}\sigma}\hat{c}_{\mathbf{k}+\boldsymbol{\pi}\sigma}\right]\end{aligned}$$

In the second passage, the sum over the full BZ was written considering that the entirety of the zone is given by all the points in the MBZ plus their conjugates obtained by a $\boldsymbol{\pi}$ shift in the flipped band. As depicted in Fig. **??**, kinetic energy is anti-periodic in $\mathbf{k}$ space by a vector $\boldsymbol{\pi}$. This anti-periodicity accounts for the minus sign arising in the third passage. The hamiltonian is then given by:

$$\hat{H} = \sum_{\mathbf{k}\in\mathrm{MBZ}}\sum_{\sigma}\hat{\Psi}^{\dagger}_{\mathbf{k}\sigma}h_{\mathbf{k}\sigma}\hat{\Psi}_{\mathbf{k}\sigma} \quad \text{being} \quad h_{\mathbf{k}\sigma} \equiv \begin{bmatrix}\epsilon_{\mathbf{k}} & -\Delta_{\sigma}\\ -\Delta_{\sigma} & -\epsilon_{\mathbf{k}}\end{bmatrix} \tag{1.5}$$

Notice: the Nambu hamiltonian is a 2×2 matrix over the MBZ – which is half the full BZ, coherently with a solution which essentially bipartites the lattice giving back a double sized unit cell.

Figure 1.3 | Pseudo-magnetic field originating from mean-field treatment of the square Hubbard hamiltonian. Here, only the $\sigma =\uparrow$ situation is plotted.

Figure 1.4 | Depiction of the AF bands $\pm E_{\mathbf{k}}$. [To be continued...]

1.3.2 Diagonalization and AF ground state

The system ground-state is obtained by the means of a Bogoliubov rotation. The hamiltonian maps onto the simple one of a spin in a magnetic field,

$$h_{\mathbf{k}\sigma} = \epsilon_{\mathbf{k}}\tau^z - \Delta_\sigma \tau^x$$

being τ^α the Pauli matrices. Then, defining

$$\hat{s}^\alpha_{\mathbf{k}\sigma} \equiv \hat{\Psi}^\dagger_{\mathbf{k}\sigma}\tau^\alpha\hat{\Psi}_{\mathbf{k}\sigma} \quad \text{and} \quad \mathbf{b}_{\mathbf{k}\sigma} \equiv \begin{bmatrix} -\Delta_\sigma \\ 0 \\ \epsilon_{\mathbf{k}} \end{bmatrix}$$

one gets:

$$\hat{H} = \sum_{\mathbf{k}\in \mathrm{MBZ}} \sum_\sigma \mathbf{b}_{\mathbf{k}\sigma}\cdot\hat{\mathbf{s}}_{\mathbf{k}\sigma} \quad \text{where} \quad \hat{\mathbf{s}}_{\mathbf{k}\sigma} = \begin{bmatrix} \hat{s}^x_{\mathbf{k}\sigma} \\ \hat{s}^y_{\mathbf{k}\sigma} \\ \hat{s}^z_{\mathbf{k}\sigma} \end{bmatrix} \tag{1.6}$$

The hamiltonian represents a system of spins subject to local magnetic fields, each tilted by an angle $\tan(2\theta_{\mathbf{k}\sigma}) = \Delta_\sigma/\epsilon_{\mathbf{k}}$, as sketched in Fig. 1.3. At any finite temperature, the ground-state of such a system is well-known. Diagonalization of each $h_{\mathbf{k}\sigma}$ is obtained trivially by a simple rotation around the y axis:

$$d_{\mathbf{k}\sigma} = W_{\mathbf{k}\sigma} h_{\mathbf{k}\sigma} W^\dagger_{\mathbf{k}\sigma}$$

where

$$d_{\mathbf{k}\sigma} = \begin{bmatrix} -E_{\mathbf{k}} & \\ & E_{\mathbf{k}} \end{bmatrix} \quad \text{and} \quad W_{\mathbf{k}\sigma} = \exp\left\{ i\frac{2\theta_{\mathbf{k}\sigma}-\pi}{2}\tau^y \right\}$$

Note that rotation is taken to be of an angle $2\theta_{\mathbf{k}\sigma} - \pi$ in order to anti-align the pseudo-spin with the magnetic field of Fig. 1.3 and thus order the eigenvalues as in $d_{\mathbf{k}\sigma}$, with the smaller one in the top-left corner of the matrix and the larger one in the bottom-right corner. The explicit form of the transformation matrix is thus

$$W_{\mathbf{k}\sigma} = \begin{bmatrix} \cos\theta_{\mathbf{k}\sigma} & -\sin\theta_{\mathbf{k}\sigma} \\ \sin\theta_{\mathbf{k}\sigma} & \cos\theta_{\mathbf{k}\sigma} \end{bmatrix} \begin{bmatrix} & -1 \\ 1 & \end{bmatrix} = \begin{bmatrix} -\sin\theta_{\mathbf{k}\sigma} & -\cos\theta_{\mathbf{k}\sigma} \\ \cos\theta_{\mathbf{k}\sigma} & -\sin\theta_{\mathbf{k}\sigma} \end{bmatrix} \tag{1.7}$$

Eigenvalues are:

$$E_{\mathbf{k}} \equiv \sqrt{\epsilon^2_{\mathbf{k}} + |\Delta_\sigma|^2} \tag{1.8}$$

Note that considering the full hamiltonian $\hat{H} - \mu\hat{N}$, the diagonalizing matrix remains the same, being

$$-\mu\hat{N} = \sum_{\mathbf{k}\in\mathrm{MBZ}} \begin{bmatrix} -\mu & \\ & -\mu \end{bmatrix} \quad \Longrightarrow \quad W_{\mathbf{k}\sigma}\left[h_{\mathbf{k}\sigma} - \mu\mathbb{I}_{2\times 2}\right] W^\dagger_{\mathbf{k}\sigma} = d_{\mathbf{k}\sigma} - \mu\mathbb{I}_{2\times 2} \tag{1.9}$$

thus for non-null chemical potential (i.e. finite doping) the eigenvalues are just shifted, $\pm E_{\mathbf{k}} - \mu$. In other words, the new bands retain the same chemical potential of the bare bands. Notice also that the presence of an absolute value makes the eigenvalues independent of the σ index. Eigenvector fermion operators are obtained simply as:

$$\hat{\Gamma}_{\mathbf{k}\sigma} = W_{\mathbf{k}\sigma}\hat{\Psi}_{\mathbf{k}\sigma} \tag{1.10}$$

The $\hat{\Gamma}$ spinor operators are effectively free fermionic spinor fields and as such must be treated.

The consequence of Eq. (1.9) is interesting by itself: within this HF solution, the gap opens always at $E = 0$. In other words, the bands sketched in Fig. 1.4 retain the same geometric features

regardless of the doping, what changes is the bands width and the gap between them. The very key point here is that, being the two bands symmetric (thus containing each half of the electronic states) and defined over the MBZ, any finite doping $\delta > 0$ will produce a metallic behaviour, imposing that the chemical potential crosses the upper band. It is widely observed and confirmed by more refined numerical procedures, however, that AF establishes an insulating phase – here only reproduced at half-filling, where the chemical potential lies within the gap. As will be detailed in 1.3.6, the commensurate nature of AF SSB at wavevector $\boldsymbol{\pi}$ of this self-consistent solution is highly unstable and atypical at finite doping [9].

1.3.3 Chemical potential and system density

The total number of electrons is given by

$$\begin{aligned} N &= \sum_{\mathbf{k}\sigma} \langle \hat{n}_{\mathbf{k}\sigma} \rangle \\ &= \sum_{\sigma} \sum_{\mathbf{k}\in \mathrm{MBZ}} \langle \hat{n}_{\mathbf{k}\sigma} + \hat{n}_{\mathbf{k}+\boldsymbol{\pi}\sigma} \rangle \\ &= \sum_{\sigma} \sum_{\mathbf{k}\in \mathrm{MBZ}} \left\langle \hat{\Gamma}^{\dagger}_{\mathbf{k}\sigma} \hat{\Gamma}_{\mathbf{k}\sigma} \right\rangle \\ &= 2 \sum_{\mathbf{k}\in \mathrm{MBZ}} \left[f\left(-E_{\mathbf{k}}; \beta, \mu\right) + f\left(E_{\mathbf{k}}; \beta, \mu\right) \right] \end{aligned} \tag{1.11}$$

being f be the Fermi-Dirac distribution at inverse temperature β and chemical potential μ,

$$f(\epsilon; \beta, \mu) = \frac{1}{e^{\beta(\epsilon-\mu)} + 1}$$

The 2 prefactor appeared because of spin degeneracy. Since the gapped bands refer to the smaller MBZ, thus exhibit the periodicity

$$E_{\mathbf{k}} = E_{\mathbf{k}+\boldsymbol{\pi}}$$

it holds equivalently

$$N = \sum_{\mathbf{k}\in \mathrm{BZ}} \left[f\left(-E_{\mathbf{k}}; \beta, \mu\right) + f\left(E_{\mathbf{k}}; \beta, \mu\right) \right] \tag{1.12}$$

as is obvious. The 2 prefactor was absorbed in doubling the integration region, MBZ $\to$ BZ. Next sections are devoted to simplify the above theoretical results in order to obtain an algorithmic estimation for the magnetization m, which is just the AF instability order parameter.

In Fig. 1.5 the density $n(\mu)$ is plotted as a function of μ. As is evident, at nearly zero temperature ($\beta \to \infty$) the system is half filled for $-\Delta < \mu < \Delta$. In order to obtain a finite doping, it must be $|\mu| > \Delta$; which means, the chemical potential needs to cross the electronic bands. This HF solution leads invariably to a rather unusual metallic AF at any finite doping.

1.3.4 Self-consistent magnetization

A convergence algorithm can be designed to find the Hartree-Fock solution to the model. Ultimately, we aim to extract m self-consistently. Since

$$\begin{aligned} m &= \frac{1}{2L_xL_y} \sum_{\mathbf{r}} (-1)^{x+y} \langle \hat{n}_{\mathbf{r}\uparrow} - \hat{n}_{\mathbf{r}\downarrow} \rangle \\ &= \frac{1}{2L_xL_y} \sum_{\mathbf{k}\in \mathrm{BZ}} \left\langle \hat{c}^{\dagger}_{\mathbf{k}\uparrow} \hat{c}_{\mathbf{k}+\boldsymbol{\pi}\uparrow} - \hat{c}^{\dagger}_{\mathbf{k}\downarrow} \hat{c}_{\mathbf{k}+\boldsymbol{\pi}\downarrow} \right\rangle \\ &= \frac{1}{2L_xL_y} \sum_{\mathbf{k}\in \mathrm{MBZ}} \left\langle \left(\hat{c}^{\dagger}_{\mathbf{k}\uparrow} \hat{c}_{\mathbf{k}+\boldsymbol{\pi}\uparrow} + \hat{c}^{\dagger}_{\mathbf{k}+\boldsymbol{\pi}\uparrow} \hat{c}_{\mathbf{k}\uparrow} \right) - \left(\hat{c}^{\dagger}_{\mathbf{k}\downarrow} \hat{c}_{\mathbf{k}+\boldsymbol{\pi}\downarrow} + \hat{c}^{\dagger}_{\mathbf{k}+\boldsymbol{\pi}\downarrow} \hat{c}_{\mathbf{k}\downarrow} \right) \right\rangle \end{aligned}$$

In the last passage, Eq. (1.4) has been used. Then magnetization can be computed simply as

$$m = \frac{1}{2L_xL_y} \sum_{\mathbf{k}\in \mathrm{MBZ}} \left[\left\langle \hat{\Psi}^{\dagger}_{\mathbf{k}\uparrow} \tau^x \hat{\Psi}_{\mathbf{k}\uparrow} \right\rangle - \left\langle \hat{\Psi}^{\dagger}_{\mathbf{k}\downarrow} \tau^x \hat{\Psi}_{\mathbf{k}\downarrow} \right\rangle \right] \tag{1.13}$$

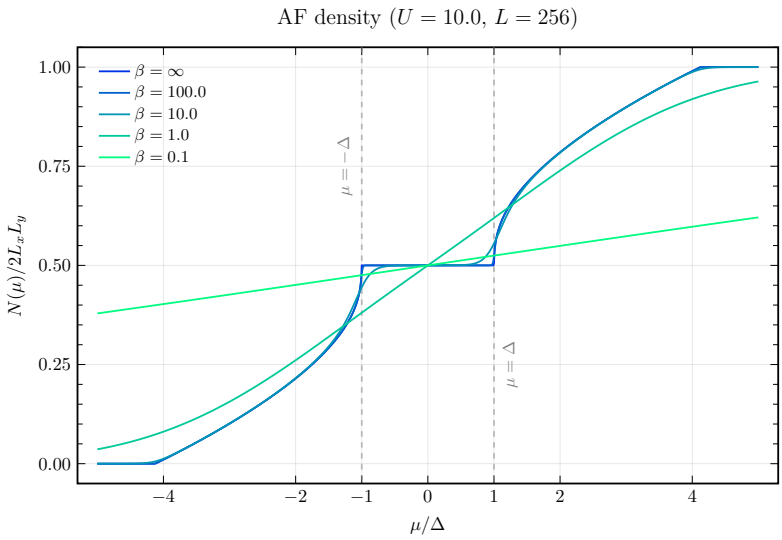

Figure 1.5 | Electronic density in the AF phase as a function of the chemical potential, measured in relation to the gap Δ, at various temperatures.

In this equation, spin expectation values appear:

$$\left\langle \hat{\Psi}^\dagger_{\mathbf{k}\sigma} \tau^x \hat{\Psi}_{\mathbf{k}\sigma} \right\rangle = \langle \hat{s}^x_{\mathbf{k}\sigma} \rangle$$

Now discussion is divided in two parts: zero temperature and finite temperature.

Zero temperature solution. For a spin system at zero temperature, the spin operator expectation value anti-aligns with the external field,

$$\langle \hat{s}^x_{\mathbf{k}\sigma} \rangle = \sin(2\theta_{\mathbf{k}\sigma})$$

(see Fig. 1.3). Now, since $\Delta_\downarrow = -\Delta_\uparrow$, it follows

$$\theta_{\mathbf{k}\uparrow} = -\theta_{\mathbf{k}\downarrow} \equiv \theta_{\mathbf{k}}$$

Then, from Eq. (1.13)

$$\begin{aligned} m &= \frac{1}{L_x L_y} \sum_{\mathbf{k}\in \mathrm{MBZ}} \sin(2\theta_{\mathbf{k}}) \\ &= \frac{1}{2L_x L_y} \sum_{\mathbf{k}\in \mathrm{BZ}} \sin(2\theta_{\mathbf{k}}) \end{aligned}$$

The last passage is due to the fact that the sum over the MBZ can be performed identically over BZ $\setminus$ MBZ and yield the same result. This is because of the lattice periodicity in reciprocal space. Then, finally:

$$m = \frac{1}{L_x L_y} \sum_{\mathbf{k}\in \mathrm{BZ}} [W_{\mathbf{k}\uparrow}]_{11} [W^\dagger_{\mathbf{k}\uparrow}]_{21} \tag{1.14}$$

where $\sin(2\theta_{\mathbf{k}}) = 2\sin\theta_{\mathbf{k}} \cos\theta_{\mathbf{k}}$ has been used. As will become clear in next section, the sudden appearance of matrix elements of W is not casual.

Finite temperature solution. At finite temperature β, discussion is analogous to the section above. Here will be treated somewhat more theoretically. Define the generic order parameter:

$$\Delta_{ij}(\mathbf{k}\sigma) \equiv \left\langle [\hat{\Psi}^\dagger_{\mathbf{k}\sigma}]_i [\hat{\Psi}_{\mathbf{k}\sigma}]_j \right\rangle$$

In last section, the relevant indices (i, j) were $(1, 2)$ and $(2, 1)$. Transform this order parameter,

$$\begin{aligned}
\Delta_{ij}(\mathbf{k}\sigma) &= \sum_{i'j'} \left\langle [\hat{\Gamma}^\dagger_{\mathbf{k}\sigma}]_{i'} [W_{\mathbf{k}\sigma}]_{i'i} [W^\dagger_{\mathbf{k}\sigma}]_{jj'} [\hat{\Gamma}_{\mathbf{k}\sigma}]_{j'} \right\rangle \\
&= \sum_{i'j'} [W_{\mathbf{k}\sigma}]_{i'i} [W^\dagger_{\mathbf{k}\sigma}]_{jj'} \left\langle [\hat{\Gamma}^\dagger_{\mathbf{k}\sigma}]_{i'} [\hat{\Gamma}_{\mathbf{k}\sigma}]_{j'} \right\rangle \\
&= \sum_{i'j'} [W_{\mathbf{k}\sigma}]_{i'i} [W^\dagger_{\mathbf{k}\sigma}]_{jj'} \delta_{i'j'} f\left([d_{\mathbf{k}\sigma}]_{i'i'}; \beta, \mu\right) \\
&= \sum_{\ell=1}^{2} [W_{\mathbf{k}\sigma}]_{\ell i} [W^\dagger_{\mathbf{k}\sigma}]_{j\ell} f\left((-1)^\ell E_{\mathbf{k}\sigma}; \beta, \mu\right) \\
&= [W_{\mathbf{k}\sigma}]_{1i} [W^\dagger_{\mathbf{k}\sigma}]_{j1} f\left(-E_{\mathbf{k}}; \beta, \mu\right) + [W_{\mathbf{k}\sigma}]_{2i} [W^\dagger_{\mathbf{k}\sigma}]_{j2} f\left(E_{\mathbf{k}}; \beta, \mu\right) \qquad (1.15)
\end{aligned}$$

In the second passage this distribution appeared because an expectation value over a gas of free Φ fermions was taken. Such an expectation value admits no off-diagonal values, hence the $\delta_{i'j'}$. The diagonal entries are precisely the definition of the Fermi-Dirac distribution for the given energy. At zero temperature and half-filling, the lower band $-E_{\mathbf{k}}$ is completely filled while the upper band $E_{\mathbf{k}}$ is empty. Substituting $f = 1$ in the first term of line (1.15), $f = 0$ in the second and summing Δ_{12} and Δ_{21} as done in Eq. (1.13), it's easy to derive the result of Eq. (1.14). At finite temperature, following the lead of the above paragraph, the antiferromagnetic instability order parameter m will be given simply by

$$m = \frac{1}{2L_xL_y} \sum_{\mathbf{k}\in \mathrm{BZ}} \sum_{\ell=1}^{2} [W_{\mathbf{k}\uparrow}]_{\ell 1} [W^\dagger_{\mathbf{k}\uparrow}]_{2\ell} f\left((-1)^\ell E_{\mathbf{k}}; \beta, \mu\right) \qquad (1.16)$$

Then: mean-field approximations yield an estimate for the magnetization at a given temperature and chemical potential just by carefully combining the elements of the diagonalizing matrix W of each Bogoliubov matrix $h_{\mathbf{k}\sigma}$.

1.3.5 The half-filled case

Consider specifically the half-filled situation. Since due to symmetry $\mu = 0$, we have the finite-temperature self-consistent equation

$$\begin{aligned}
m &= \frac{1}{L_xL_y} \sum_{\mathbf{k}\in \mathrm{MBZ}} \sin(2\theta_{\mathbf{k}}) \left[f\left(-E_{\mathbf{k}}; \beta, 0\right) - f\left(E_{\mathbf{k}}; \beta, 0\right)\right] \\
&= \frac{1}{2L_xL_y} \sum_{\mathbf{k}\in \mathrm{MBZ}} \frac{\Delta}{\sqrt{\epsilon^2_{\mathbf{k}} + \Delta^2}} \tanh\left(\frac{\beta}{2}\sqrt{\epsilon^2_{\mathbf{k}} + \Delta^2}\right)
\end{aligned}$$

Recalling that $m = \Delta/U$, the above equation becomes in thermodynamic limit $L \to \infty$

$$\frac{1}{U} \simeq \frac{1}{2} \int_{\mathrm{MBZ}} \frac{\mathrm{d}\mathbf{k}}{(2\pi)^2} \frac{1}{\sqrt{\epsilon^2_{\mathbf{k}} + \Delta^2}} \tanh\left(\frac{\beta}{2}\sqrt{\epsilon^2_{\mathbf{k}} + \Delta^2}\right)$$

Substitute the momentum integral with an integral over energies, in the low temperature limit, $\beta \to \infty$ (thus approximate the hyperbolic tangent with 1)

$$\frac{1}{U} \simeq \frac{1}{2} \int_{\mathrm{bands}} \frac{\mathrm{d}\epsilon \rho(\epsilon)}{\sqrt{\epsilon^2 + \Delta^2}}$$

[To be continued...]

1.3.6 Instability of the commensurate AF solution and atypical metallic bands

A key point to be discussed is the known instability of the AF HF solution of the EHM. As is thoroughly discussed in [9], the solution we presented above is only stable at half-filling, becoming

hardly unstable at infinitesimal doping. This is due to the commensurate nature of the established AF phase: we impose SSB to take place at wavevector $\boldsymbol{\pi}$, shrinking the BZ to exactly half its size and giving back on the newly defined MBZ two bands $\pm E_{\mathbf{k}}$. This procedure actually works well for the half-filled case: the magnetization essentially depends on the scattering rate between points on the FS connected by a $\boldsymbol{\pi}$ vector. The half filled case, taking advantage of the natural nesting property of the bare bands,

$$\forall \mathbf{k} \in \partial\text{MBZ} : \ \epsilon_{\mathbf{k}} = \epsilon_{\mathbf{k}+\boldsymbol{\pi}}$$

(being ∂MBZ the boundary of the MBZ) exhibits a magnetization at infinitesimal interaction. For a many body state resulting from continuous SSB, to establish a given phase means to show the presence of a stable gapless Goldstone mode associated to the broken symmetry. Such a Goldstone mode is essentially a sharp peak at zero frequency for some dressed response function. For the AF phase, it follows from the reduced $\mathrm{U}^z(1)$ rotational symmetry and is related to the transverse pseudospin-pseudospin response function,

$$\tilde{\chi}_{\hat{\mathbf{S}}^-\hat{\mathbf{S}}^+}(\mathbf{k},\omega) = \frac{\chi_{\hat{\mathbf{S}}^-\hat{\mathbf{S}}^+}(\mathbf{k},\omega)}{1 - U\chi_{\hat{\mathbf{S}}^-\hat{\mathbf{S}}^+}(\mathbf{k},\omega)}$$

As is shown in [9], for the commensurate AF SSB at wavevector $\boldsymbol{\pi}$ the condition for the presence of a stable gapless mode reduces to a 2×2 matrix equation,

$$\mathbb{I}_{2\times 2} - U\left[\chi_{\hat{\mathbf{S}}^-\hat{\mathbf{S}}^+}(\boldsymbol{\pi},0)\right] \geq 0$$

with $\left[\chi_{\hat{\mathbf{S}}^-\hat{\mathbf{S}}^+}(\boldsymbol{\pi},\omega)\right]$ the response function matrix obtained by considering a matrix response function for a two-sites unit cell. Considering the eigenvalue of largest amplitude of the matrix λ_δ at filling δ, the one most prone to instabilities, it is found that

$$\begin{aligned}
\lambda_0(\mathbf{k}\to\boldsymbol{\pi},0) &= \frac{1}{U} && \text{(half filling)}\\
\lambda_\delta(\mathbf{k}\to\boldsymbol{\pi},0) &= \frac{1}{U} + \frac{2\epsilon_{\mathrm{F}}}{\Delta}N(\epsilon_{\mathrm{F}}) && \text{(finite doping)}
\end{aligned}$$

The reason for the distinction above is the intrinsic metallic nature of the system for infinitesimal doping. At half-filling the system is an insulator, therefore no Fermi energy is defined, as well as no FS. Evidently this implies

$$\begin{aligned}
1 - U\lambda_0(\mathbf{k}\to\boldsymbol{\pi},0) = 0 \quad &\text{(half filling)} \quad \Longrightarrow \quad \text{stable Goldstone mode}\\
1 - U\lambda_\delta(\mathbf{k}\to\boldsymbol{\pi},0) < 0 \quad &\text{(finite doping)} \quad \Longrightarrow \quad \text{unstable Goldstone mode}
\end{aligned}$$

For any finite doping, the commensurate AF phase becomes unstable and is destroyed by transverse spin fluctuations. Nevertheless, for the sake of completeness, we will study the metallic AF also at finite doping.

1.3.7 Hartree-Fock algorithm results in reciprocal space

The above sections offer a self-consistency equation for the magnetization m; W is determined by m indeed. Then a self-consistent algorithm to search for a self consistent estimate for m may be sketched, following the general idea of Sec. **??**:

0. Algorithm setup: initialize a counter $i = 1$ and choose:
   - the local repulsion U/t or equivalently the hopping amplitude t/U;
   - the coarse-graining of the BZ, which is, fix L_x and L_y. Then
     $$k_x = 2\pi n_x/L_x \qquad k_y = 2\pi n_y/L_y$$
     where $-L_j/2 \leq n_j \leq L_j/2$, $n_j \in \mathbb{Z}$;
   - the density n or equivalently the doping $\delta \equiv n - 0.5$;
   - the inverse temperature β;

- the number of iterations $p \in \mathbb{N}$;
- the mixing parameter $g \in [0, 1]$;
- the tolerance parameters $\Delta_m, \Delta_n \in \mathbb{R}$ (respectively for magnetization and density);

1. Select a random starting value $m_0 \in [0, 1]$;
2. For each slot of the BZ, initialize the appropriate 2×2 matrix $h_{\mathbf{k}\uparrow}$ as in Eq. (1.5);
3. For the given hamiltonian, find the optimal chemical potential μ as follows:
   a) Diagonalize $h_{\mathbf{k}\uparrow}[m_0, U]$ and obtain its eigenvalues $\pm E_{\mathbf{k}}[m_0, U]$;
   b) Define the function of the chemical potential μ,
   $$\delta n(\mu; \beta, m_0, U) \equiv 2 \left[f\left(-E_{\mathbf{k}}[U, m_0]; \beta, \mu\right) + f\left(E_{\mathbf{k}}[U, m_0]; \beta, \mu\right)\right] - n$$
   c) Find the root of δn,
   $$\delta n(\mu_0) = 0$$
   Then μ_0 is the chemical potential which, at magnetization m_0, realizes the best approximation of density n;
4. Diagonalize the matrix $h_{\mathbf{k}\uparrow}$ and obtain $d_{\mathbf{k}\uparrow}$;
5. Compute m using Eq. (1.16) with chemical potential μ_0 and update the counter, $i \to i + 1$;
6. Check if $|m - m_0| \leq \delta_m$:
   - If yes, halt;
   - If not: check if $i > p$
     - If yes, halt and consider choosing better tolerance and model parameters;
     - If not, define
     $$m_0 = gm + (1 - g)m_0$$
     (logical assignment notation used) and repeat from step 2.

The algorithm sketched hereby was ran with the following setup:

```
UU = [U for U in 0.5:0.5:20.0]        # Local repulsions
LL = [256]                            # Lattice sizes
dd = [d for d in 0.0:0.05:0.45]       # Dopings
bb = [100.0, Inf]                     # Inverse temperatures
p = 100                               # Max number of iterations
dm = 1e-4                             # Tolerance on magnetization
dn = 1e-2                             # Tolerance on density
g = 0.5                               # Mixing parameter
```

In Fig. 1.6 plots at $\beta = 100$ of the magnetization m is reported. As is evident in Fig. 1.6a, doping disrupts AF ordering; the horizontal asymptote lowers as δ gets bigger, a mere consequence of the fact that the free space at each single-particle state in k-space shrinks as density increases; also, for $\delta > 0$, a finite magnetization m exists only for $U \geq U_c[\delta]$ (a critical value parametrically dependent on doping). Fig. 1.6b shows the dependence of magnetization on doping at various fixed local repulsions U: once again, to dope the material disrupt AF ordering. Identical analysis have been performed for different temperatures, leading to analogous results as long as $\beta \gtrsim 10$ and to $m \simeq 0$ for higher temperatures (predictably).

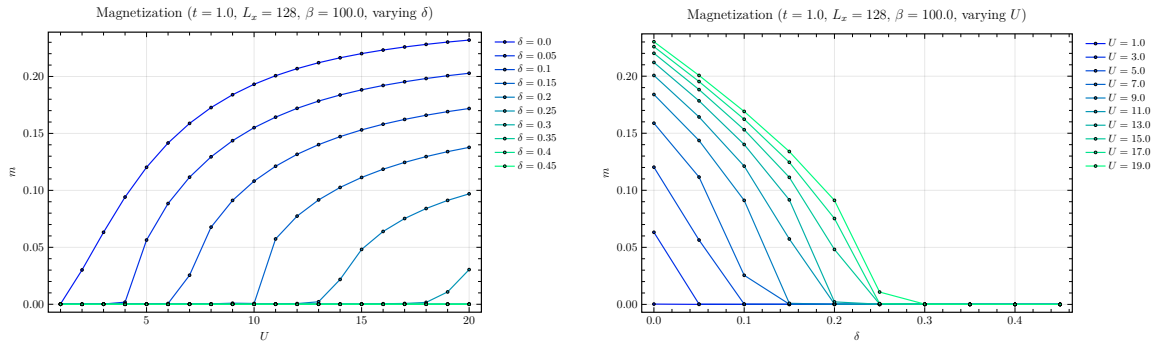

a | Local repulsion U/t depencence. b | Doping $\delta = n - 0.5$ dependence.

Figure 1.6 | Plots of the zero-temperature AF instability order parameter m as a function of both the local repulsion U/t (Fig. 1.6a) and the doping $\delta = n - 1/2$ (Fig. 1.6b).

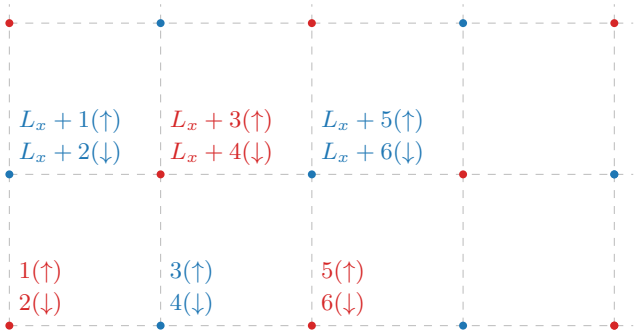

Figure 1.7 | Schematics of the site ordering on a square lattice performed by sweeping along rows. Left-bottom side is one corner of the lattice. Red sites are characterized by $x+y$ being odd, blue sites by being even. The number reported near to each site is the α entry in the matrix representation for a finite square lattice.

1.3.8 An alternative (less efficient) real-space approach

The theoretical derivation of the above paragraphs offers a simple description of the system anti-ferromagnetic instability as the instauration of a ground-state of quasiparticles. Here a self-consistent algorithmic extraction of the expected magnetization is presented, following [8]. Note that this algorithm is by far the least efficient, being performed in real space with dimensional exponential scaling in terms of computational time. It is here presented just for completeness as an alternative derivation. This algorithm can become useful for simulations not preserving space-translational invariance, e.g. introducing some degree of disorder. Consider a square lattice of $L_x \times L_y$ sites: the hamiltonian will be a matrix of dimension $2L_xL_y \times 2L_xL_y$,

$$[\hat{H}]_{(\mathbf{r}\sigma)(\mathbf{r}'\sigma')} = \langle\Omega|\hat{c}_{\mathbf{r}\sigma}\hat{H}\hat{c}^{\dagger}_{\mathbf{r}'\sigma'}|\Omega\rangle$$

For simplicity, in the following $D \equiv 2L_xL_y$. In this context, the following convention is used: the rows/column index entry $\alpha = (\mathbf{r}\sigma)$ is associated to a specific site $\mathbf{r} = (x, y)$ and spin σ through the relation

$$\alpha = 2j_{\mathbf{r}} - \delta_{\sigma=\uparrow} \quad \text{where} \quad j_{\mathbf{r}} = x + (y-1)L_x$$

Let me break this through. For each site $\mathbf{r}$, two sequential indices are provided ($2j_{\mathbf{r}} - 1$, hosting spin $\uparrow$, and $2j_{\mathbf{r}}$, hosting spin $\downarrow$). $j_{\mathbf{r}}$ just orders the site rows-wise. This way, $(x, 1)$ is assigned to $j_{(x,1)} = x$, while its NN one site above $(x, 2)$ is assigned to an entry shifted by L_x, $j_{(x,2)} = x + L_x$. This is just a way of counting the site of a finite square lattice by sweeping along a row and then moving to the row above. Fig. 1.7 reports a scheme of the used site ordering.

Within this convention, matrix elements $H_{\alpha\beta}$ are defined by:

- If $\sigma = \sigma'$ and $\mathbf{r}$, $\mathbf{r}'$ are NN, the matrix entry is $-t$. In terms of the used greek indices, α and β satisfy said requirement if $|\alpha - \beta| = 2$ (horizontal hopping) or $|\alpha - \beta| = 2L_x$ (vertical hopping). Along column α of the hamiltonian matrix, the elements $-t$ appear at positions

$$(\alpha \pm 2L_x) \mod D \quad \text{and} \quad (\alpha \pm 2) \mod D$$

- If $\mathbf{r} = \mathbf{r}'$ and $\sigma = \sigma'$ (along the diagonal), the local interaction with the mean field is given by the matrix element

$$-mU \times (-1)^{x+y} \times (-1)^{\delta_{\sigma=\downarrow}}$$

Starting from a given entry α, $j_{\mathbf{r}}$ is retrieved simply by $j_{\mathbf{r}} = \lfloor \alpha/2 \rfloor$, and then

$$x + y = (j_{\mathbf{r}} + 1) - \left\lfloor \frac{j_{\mathbf{r}}}{L_x} \right\rfloor (L_x - 1)$$

Then the $j_{\mathbf{r}}$-th 2×2 block along the diagonal will be given by

$$(-1)^{x+y} \underbrace{\begin{bmatrix} -mU & \\ & mU \end{bmatrix}}_{\mathcal{B}}$$

Note that the resulting block diagonal contribution to the hamiltonian is shaped like follows (assume L_x to be even):

$$\begin{array}{c} \\ 1 \\ 2 \\ \vdots \\ L_x - 1 \\ L_x \\ L_x + 1 \\ L_x + 2 \\ \vdots \end{array} \begin{array}{c} \begin{array}{cccccccc} 1 & 2 & \cdots & L_x - 1 & L_x & L_x + 1 & L_x + 2 & \cdots \end{array} \\ \begin{bmatrix} \mathcal{B} & & & & & & & \\ & -\mathcal{B} & & & & & & \\ & & \ddots & & & & & \\ & & & \mathcal{B} & & & & \\ & & & & -\mathcal{B} & & & \\ & & & & & -\mathcal{B} & & \\ & & & & & & \mathcal{B} & \\ & & & & & & & \ddots \end{bmatrix} \end{array}$$

Along the same row, on the diagonal the 2×2 blocks $\mathcal{B}$ alternate signs; changing row (in the example above, at positions $L_x, L_x + 1$), due to the anti-ferromagnetic configuration of local mean-fields, an additional -1 is included. If L_x is taken to be odd, the diagonal blocks just alternate signs all the way.

These prescriptions allow to build from scratch the hamiltonian matrix. After that, diagonalization provides D orthonormal eigenvectors $\mathbf{v}^\ell \in \mathbb{C}^{D \times D}$ with $\ell = 1, \cdots, D$, each associated to a precise eigenvalue $\epsilon^\ell \in \mathbb{R}$. At equilibrium, electrons will fill up the energy eigenstates according to,

$$\langle \hat{n}_{\mathbf{r}\sigma} \rangle = \sum_{\ell=1}^{D} \left| v_\alpha^\ell \right|^2 f(\epsilon^\ell; \beta, \mu) \quad \text{where} \quad \alpha = (\mathbf{r}\sigma)$$

For a fixed filling $n = N/D$, the chemical potential must satisfy

$$\begin{aligned} n &= \frac{1}{D} \sum_{\mathbf{r}\sigma} \langle \hat{n}_{\mathbf{r}\sigma} \rangle \\ &= \frac{1}{D} \sum_{\mathbf{r}\sigma} \sum_{\ell=1}^{D} \left| v_\alpha^\ell \right|^2 f(\epsilon^\ell; \beta, \mu) \\ &= \frac{1}{D} \sum_{\ell=1}^{D} f(\epsilon^\ell; \beta, \mu) \end{aligned}$$

since the $\mathbf{v}^\ell$ eigenvectors are orthonormal. The chemical potential for the half-filled model is already known to be

$$\mu\big|_{n=1/2} = -\frac{U}{2}$$

as evident from Eq. (1.3). Average magnetization is then given by

$$\begin{aligned} m &= \frac{1}{D}\sum_{\mathbf{r}}(-1)^{x+y}\left[\langle\hat{n}_{\mathbf{r}\uparrow}\rangle - \langle\hat{n}_{\mathbf{r}\downarrow}\rangle\right] \\ &= \frac{1}{D}\sum_{\lambda=1}^{D/2}(-1)^{(\lambda+1)-\lfloor\lambda/L_x\rfloor(L_x-1)}\sum_{\ell=1}^{D}\left[\left|v^\ell_{2\lambda-1}\right|^2 - \left|v^\ell_{2\lambda}\right|^2\right] f(\epsilon^\ell;\beta,\mu) \end{aligned} \tag{1.17}$$

since $\mathbf{r}\uparrow$ is associated to an odd index entry, while $\mathbf{r}\downarrow$ to the following even entry. The associated HF algorithm is identical to the one presented in Sec. 1.3.7, with the following substitutions:

2. Initialize the hamiltonian matrix $H_{\alpha\beta}$ matrix according to the initialized m_0 and the site indexing rules of Fig. 1.7;

4. Diagonalize the matrix associated to the operator $\hat{H}_{\alpha\beta} - \mu\hat{N}$ collecting the $\mathbf{v}^\ell$ eigenvectors;

5. Compute m using Eq. (1.17) and update the counter, $i \to i+1$;

Bibliography

[1] Daniel P. Arovas et al. "The Hubbard Model". In: *Annual Review of Condensed Matter Physics* 13.Volume 13, 2022 (2022), pp. 239–274. ISSN: 1947-5462. DOI: https://doi.org/10.1146/annurev-conmatphys-031620-102024. URL: https://www.annualreviews.org/content/journals/10.1146/annurev-conmatphys-031620-102024.

[2] Zhangkai Cao et al. "Dominant p-wave pairing induced by nearest-neighbor attraction in the square-lattice extended Hubbard model". In: *Phys. Rev. B* 111 (2 Jan. 2025), p. 024509. DOI: 10.1103/PhysRevB.111.024509. URL: https://link.aps.org/doi/10.1103/PhysRevB.111.024509.

[3] Piers Coleman. *Introduction to Many-Body Physics*. Cambridge University Press, 2015.

[4] Michele Fabrizio. *A Course in Quantum Many-Body Theory*. Springer, 2022.

[5] Gabriele Giuliani and Giovanni Vignale. *Quantum Theory of the Electron Liquid*. Cambridge University Press, 2005.

[6] Giuseppe Grosso and Giuseppe Pastori Parravicini. *Solid State Physics*. Second Edition. Academic Press, 2014.

[7] J. E. Hirsch. "Two-dimensional Hubbard model: Numerical simulation study". In: *Phys. Rev. B* 31 (7 Apr. 1985), pp. 4403–4419. DOI: 10.1103/PhysRevB.31.4403. URL: https://link.aps.org/doi/10.1103/PhysRevB.31.4403.

[8] Robin Scholle et al. "Comprehensive mean-field analysis of magnetic and charge orders in the two-dimensional Hubbard model". In: *Phys. Rev. B* 108 (3 July 2023), p. 035139. DOI: 10.1103/PhysRevB.108.035139. URL: https://link.aps.org/doi/10.1103/PhysRevB.108.035139.

[9] Avinash Singh and Zlatko Tešanović. "Collective excitations in a doped antiferromagnet". en. In: *Physical Review B* 41.1 (Jan. 1990), pp. 614–631. ISSN: 0163-1829, 1095-3795. DOI: 10.1103/PhysRevB.41.614. URL: https://link.aps.org/doi/10.1103/PhysRevB.41.614 (visited on 12/12/2025).